ISSN PRINT 2319 1775 Online 2320 7876
Research paper  UGC CARE Listed ( Group -I) Journal Volume 10, Iss 4, 2021

# Role of Organosulphur acid of the Conductance of PANI-Computational and Physico-Chemical Studies

**A. Ananda Jebakumar**

Department of Chemistry, Government Polytechnic College for Women, Madurai, Tamilnadu, India-625011

**Abstract**

Sulphur acids have much different behaviour than a carboxylic acid. Sulphur has a different role due to its bulkiness and electron donating ability. This work has the composites of PANI with sulphur acids. The behaviour of PANI in the presence of sulphur acid is studied by DFT, TDFT, spectra and conductance for four different compositions. Conductance of PANI is reduced by composting by sulphur acids. The order of conductance of composites is PANI-BCG > PANI-PRR > PANI-SA. The role of altering the conductance is electronic over structural. The conductance is by hoping of $H^+$ in the field created by the counterion chloride and polymer.

Keywords: PANI, Composite, DFT, spectral, Conductance

## 1. Introduction

A major role of research in electrochemistry is to design a conductance of polymers [1]. Such alteration can be done through composing also [2]. Compositing gives the role of a compound on the characters of one another [3]. Conducting polymer based composites have attracted significant interest in recent research due to their remarkably enhanced electrical, electrochemical, and dielectric properties, which allow for their use in electrochemical sensors [4], stretchable electronics [5], supercapacitors [6], batteries and so on [7]. A simple class of conductance polymer is polyaniline (PANI) [8]. PANI has many forms the basic form is emeraldine base which is a neutral polymer derived from aniline, has hetero atom [9]. By the addition of HCl to the emeraldine base and protonated on its nitrogen its conductance

  

raised to a greater extent [10] which is emeraldine salt [11] and mentioned here as PANI. It is worthwhile to mention here an insulator becomes a conductor due to slight modification [12]. Another role of compositing is to study the role of one of the components on another and accomplishing the mechanism involved in the process [13]. Likewise, the compositing of PANI leads to understanding the mechanism of conductance of it [14]. For a better understanding of a physic-chemical process along with experimental computation has a major role in it [15]. Among the computational DFT played a major role [16]. Composing using heteroatoms are more trivial especially sulphur has a major role in it [17]. Here the DFT and experimental study of PANI composites of Patton & Reeder's reagent (PANI-PRR), sulphamic acid (PANI-SA) and bromocresol green (PANI-BCG). Computations are performed to get information about thermodynamic stability, structural parameters, dipole moment, charge density, HOMO, LUMO, frontier orbitals, spectra, TDDFT and NLO. The composites are synthesised, characterisation by FTIR, UV-VIS, fluorescence and DC conductance for the composites of 100, 80, 67,57and 50% of PANI by wt.

## 2. Experimental

### *2.1 Synthesis of PANI*

All the chemicals used were of AR grade obtained from Merk, India and used as such. 10 g of aniline and 30.6 g of ammoniumperdisulphate were dissolved in 1M 250ml HCl separately and cooled them at 18°C. Ammoniumperdisulphate solution was added dropwise to the aniline solution with constant stirring for about 50 minutes. The content was kept aside for 12 hours and washed with water containing small amount of acetone. Then the content was filtered, dried at 80$^{o}$C for 8 hours and stored in a polyethylene container. Water was used as solvent. The yield is 58%. Basic unit weight is 92. The percentage doping of HCl in PANI was measured by titrating a known amount of PANI with standard alkali.

  

### *2.2 Synthesis of Composites*

Slurry was prepared by 400 mg of ES and 100 mg of CYSHC 4 ml in DMSO for using mortar and pestle. The content was dried at 70 $^{o}$C for 24 hrs. Weight loss method was employed to check the complete removal of DMSO from the mixture. The composite was powdered and stored in a polyethylene container. The same procedure was repeated with 200, 300 and 400 mg of CYSHC and amino acids. The spectral studies used 80% PANI.

### *2.3 Computation*

DFT studies were performed by B3LYP/ 6-31G** basis set in gas phase at 25 °C using firefly software [18] in i7 computer. TDDFT calculations were done using ORCA programme [19] by B3LYP/PBE0. Due to higher computational cost, the modeling studies were carried for each one unit of phenyl and phenylene rings for ES and its composites.

### *2.4 Equipment*

DC conductance was studied in Four Probe SES-Model DFP-RM. IR spectra were recorded in JASCO FT/IR-4600, UV-VIS in JASCO V-650 (DMSO Solvent) and Luminescence in Perkin Elmer, LS 45, excitation at 380 nm (DMSO Solvent).

### *2.5 Analysis*

Regression analysis was carried out for conductance studies. The equations used were; for ideal-y = $y_0$+ax; for real- y = $y_0$+ax+b$x^2$. The ideal behaviour means expected. Pearson's correlation coefficients for ideal and real behaviours were calculated using software SPSS 16 [20].

## 3. Results and discussion

This study consists of three sulphur acids viz. Patton & Reeder's reagent (PRR), sulphamic acid (SA) and bromocresol green(BCG). Due to higher computational cost only experimental studies were done for PANI-BCG. Among them, PRR has hydroxy, carboxylic

  

acid and azo groups along with sulphonic acid group. On the other hand, sulphamic acid is a simple molecule.

### 3.1 Stability and Structure

The structure and stability value of PANI-PRR and PANI-SA is given Fig. 1 and structural parameters are given in Table 1. Concerning thermodynamic stability, PANI-SA is about 5.5 times more stable than PANI-PRR. This may be due to a higher steric effect caused by PRR in PANI-PRR over SA to the PANI-SA molecule. It has been expected that the higher difference in the thermodynamic stability between PANI-SA and PANI-PRR may reflect in their geometrical parameters. But there is no significant difference in the bond length, bond angle and dihedral angle between PANI-PRR and PANI-SA. The dihedral angle $C_{2'}$-$H_{1'}$-$N_1$-$C_2$ explains that the approach angle of $H_{1'}$-$Cl_{2'}$ towards the PANI has increased by 25 and 24% respectively for PANI-PRR and PANI-SA from PANI. Except for the approach of $H_{1'}$-$Cl_{2'}$, there is no markable change caused in the geometry of PANI by PRR and SA. The stability and geometry infer that the conductance of PANI-SA is higher than PANI-PRR.

### 3.2 Charge Density

Table 2 has the charge density of this system. Here also no significant difference between PANI-PRR and PANI-SA is noted. In general the charges on $H_{1'}$ and $Cl_{2'}$ are decreased by 5.2 and 9.5% respectively compared to PANI. This implies that the binding of $H_{1'}$-$Cl_{2'}$ is weaker with PANI in the PANI-PRR and PANI-SA system when compared to PANI. The same trend is reflected in other charge densities. Charge density reveals that there is no significant difference in the conductance between PANI-SA and PANI-PRR.

### 3.3 Dipole moment

The dipole moment values are given in Table 3. The total dipole moment of PANI-SA and PANI- PRR are lesser by 5.3 and greater by 8.9 % over PANI. Both the systems have

  

higher dipole moment along *x* and *z*-directions and lower along *y*-direction than PANI. The polarisation of PANI-PRR and PANI-SA are along *z*-and *y*-directions. Thus, there is a reorientation in the dipole moment direction, which is observed for PANI-PRR from PANI. The higher dipole moment favours the conductance in PANI-PRR and change of dipole axis may retard the same.

**3.4 Molecular Orbital**

Fig. 2 has the molecular orbital diagrams of this system. MO diagrams of PANI-SA and PANI-PRR are the mere combination of PANI and PRR or SA with a slight deviation. For PRR, the HOMO and LUMO (Fig.3) involves nitrogen atom. In the case of SA, the HOMO is predominantly of oxygen and LUMO has sulphur atom. For PANI-PRR and PANI-SA, the LUMO resembles PANI and the HOMO involves the PRR, SA and PANI. Stable HOMO and LUMO of PANI-SA may hamper its conductance over PANI-PRR.

**3.5 TDDFT**

The TDDFT data are given in Table 4. Due to a bigger size, TDDFT computation was not performed for PANI-PRR. PANI-SA has one peak at a visible region and two peaks at the UV region. The visible transition is like PANI and has redshift while the UV transition at 297 nm is the combination of charge transfer transition along with transition within PANI. Another UV transition at 309 nm is from HOMO-7→LUMO. The HOMO of PANI and PANI-PRR/ PANI-SA have comparable energies, while the LUMO of PANI-PRR and PANI-SA are 40.3 and 16.3% more stable than PANI respectively. The optical band gap favours the conductance of PANI-SA over PANI.

**3.6 Frontier Molecular Orbital**

Details about the title are given in Table 5. Based on the bandgap the stability is of the order PANI-PRR (-38.9%) < PANI-SA (-2.8%) < PANI (0%). The lower stability of PANI-

  

PRR may be due to the steric effect caused by PRR. The above parameters explain that PANI-SA is more stable and PANI-PRR is highly conductive.

### 3.7 Polarizability

Table 6 has polarizability values. The polarisation of the PANI-PRR and PANI-SA are higher than PANI. PANI-PRR has a very high third order polarisation than PANI-SA. The order of polarizability for the composites is © > ⟨ > ®. The optical self-focusing effect and expected conductance are higher in PANI-PRR over PANI-SA.

### 3.8 Spectra

All the experimental IR have peaks among 1498 $cm^{-1}$ and 1582$cm^{-1}$ are attributed for benzenoid, quinonoid ring stretching and the peak at 1298 $cm^{-1}$ is due to the secondary aromatic amine and 1135 $cm^{-1}$ is for $NH^{+}$ structure in ES. The computed IR has strong absorbance at 2291 and 2745 $cm^{-1}$ due to the azomethine group present in the ring structure at the gas phase. UV-VIS of PANI-PRR has two peaks, each one is visible and UV regions. The visible peak may be the combination of n→π* and π →π* transitions and absorption in the UV region is due to ∫→∫*. The experimental optical band gap order of conductance is PANI-BCG > PANI-SA > PANI-PRR. The lower optical band gap of PANI-BCG may be due to its dye nature. Fluorescence spectra of PANI-PRR have distinct behaviour than others and intensity of characteristic peak around 780 nm reveals that PANI-SA has higher conductance in this group. PANI-PRR and PANI-BCG have emission in green and red regions, while PANI-SA in violet and red regions.

### 3.9 Conductance

Table 7 has the values of conductance. The order of parameters a, b and x are PANI-BCG > PANI-PRR > PANI-SA. The conductance of PANI-SA is greater than PANI-PRR and PANI-BCG. This may be due to the multifunctional and bulky nature of PRR and BCG,

  

which can retard the intermolecular charge carrier transition in the PANI [21]. Further, the higher molecular weight of PRR and BCG may cause dilution effect on PANI.

## 4. Conclusion

In this work, the effect of sulphur acids on the conductance of PANI was observed by computation and experimental studied. The conductance is due to the hoping of the proton due to the field generated between the polymer chain and counter chloride ion. PANI-Sulphur acid composites, the steric effect, multi-functional nature and dilution effects retard the conductance. Dye does not affect the conductance.

## Reference

1. Jürgen Heinze, Bernardo A. Frontana-Uribe, and Sabine Ludwigs' (2010), Electrochemistry of Conducting Polymers—Persistent Models and New Concepts, Chem. Rev 110, 8, 4724–4771.
2. Enas M.Ahmed (2015) Hydrogel: Preparation, characterization, and applications: A review Journal of Advanced Research 6, 2,105-121
3. Shalini Mohanty B.C. Routara R.K. Bhuayan (2017) Experimental investigation of machining characteristics for Al-SiC12% composite in Electro-discharge machining, Materials today proceedings, 4, 8, 8778-8787
4. Krishna C.Persaud, (2005) Polymers for chemical sensing material today, 8, 4, April, 38-44
5. Daniel Félix Fernandes, Carmel Majidi and Mahmoud Tavakoi (2019) Digitally printed stretchable electronics: a review, J. Mater. Chem. C, 7, 14035-14068
6. Research progress on conducting polymer based supercapacitor electrode materials Author links open overlay panelQiufengMeng[abc]KefengCai[a]YuanxunChen[a]LidongChen, Nano Energy Volume 36, June 2017, Pages 268-285
7. Dong Zhou' Devaraj Shanmukaraj' Anastasia Tkacheva, Michel Armand, Guoxiu Wang, (2019) Polymer Electrolytes for Lithium-Based Batteries: Advances and Prospects, 5, chem, 9, 12 , 2326-2352,.
8. Jolly Bhadra, Asma Alkareem & Noora Al-Thani, (2020) A review of advances in the preparation and application of polyaniline based thermoset blends and composites Journal of Polymer Research, 27, 122
9. Souhila Abaci, Belkacem Nessark & Farid Riahi, (2014) Preparation and characterization of polyaniline+$TiO_2$ composite films Ionics, 20, 1693–1702
10. Imene Bekri-Abbes & Ezzeddine Srasra, (2011) Investigation of structure and conductivity properties of polyaniline synthesized by solid–solid reaction Journal of Polymer Research 18, 659–665

11. Marcelo M. Nobrega, Klester S. Souza, Gustavo F. S. Andrade, Pedro H. C. Camargo, and Marcia L. A. Temperini, (2013), Emeraldine Salt Form of Polyaniline as a Probe Molecule for Surface Enhanced Raman Scattering Substrates Excited at 1064 nm J. Phys. Chem. C 117, 35, 18199–18205
12. Karim Khan, Ayesha Khan Tareen, Muhammad Aslam, Renheng Wang, Yupeng Zhang, Asif Mahmood, Zhengbiao Ouyang, Han Zhang and Zhongyi Guo, (2020) Recent developments in emerging two-dimensional materials and their applications J. Mater. Chem. C**,** ,8, 387-440
13. Zhangwei Chen, Ziyong Li, Junjie Li, Chengbo Liu, Changshi Lao, Yuelong Fu, Changyong Liu, Yang Li, Pei Wang, Yi He, (2019) 3D printing of ceramics: A review Journal of the European Ceramic Society 39, 4, 661-687
14. Syed Khasim, (2019) Polyaniline-Graphene nanoplatelet composite films with improved conductivity for high performance X-band microwave shielding applications Results in Physics 12, 1073-1081
15. Ryo Nagai, Ryosuke Akashi & Osamu Sugino (2020) Completing density functional theory by machine learning hidden messages from molecules, Computational Materials, 6, 43.
16. Giuseppe Felice Mangiatordi, Eric Brémond, and Carlo Adamo, (2012) J. Chem. Theory Comput, 8, 9, 3082–3088
17. Sheng S. Zhang, (2015) Heteroatom-doped carbons: synthesis, chemistry and application in lithium/sulphur batteries **,** Inorg. Chem. Front.**, 2**, 1059-1069
18. Granovsky, AA Baldridge, KK Boatz, JA Elbert, ST Gordon, MS Jensen, JH Koseki, S Matsunaga, N Nguyen, KA Su, S Windus, TL Dupuis, M & Montgomery, (1993) JA Journal of computational chemistry, 14, 11, 1347-136
19. Neese, F (2012) 'The ORCA program system', WIREs Computational Molecular Science, 2, 1, 73-78.
20. Sabine Landau and Brian S. Everitt, (2014), A Handbook of Statistical Analyses using SPSS, Chapman & Hall/CRC Press
21. Bai, H & Shi, G (2007), 'Gas Sensors Based on Conducting Polymers', Sensors, 7, 3, 267-307

ISSN PRINT 2319 1775 Online 2320 7876
Research paper  UGC CARE Listed ( Group -I) Journal Volume 10, Iss 4, 2021

**Figure 1:Structure and Thermodynamic Stability**

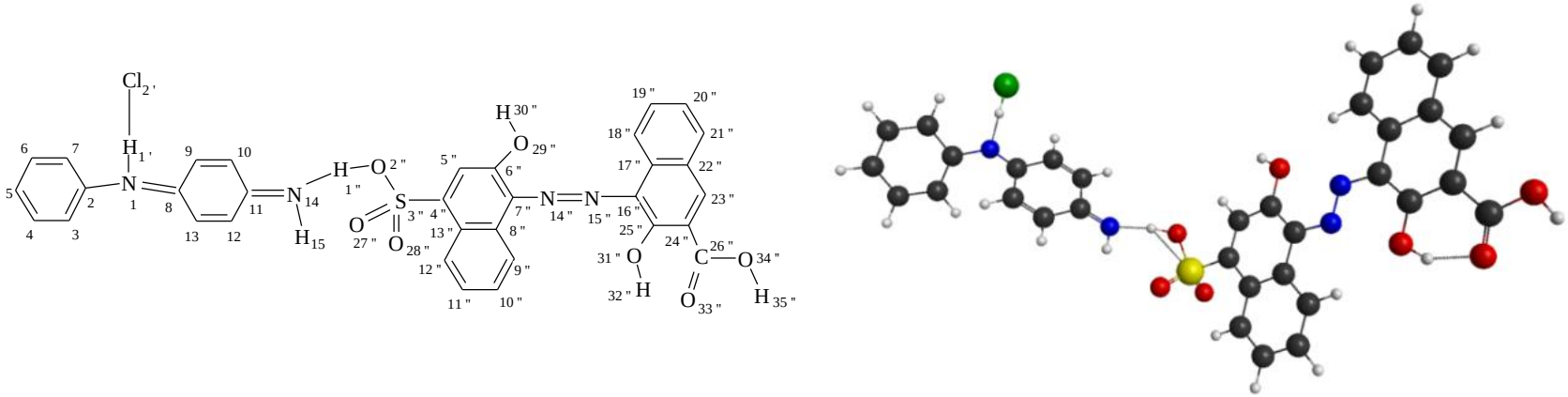

**ES-PRR**

**(**ES-PRR- (ES+ PRR) = -74.7742 kJ/mole)

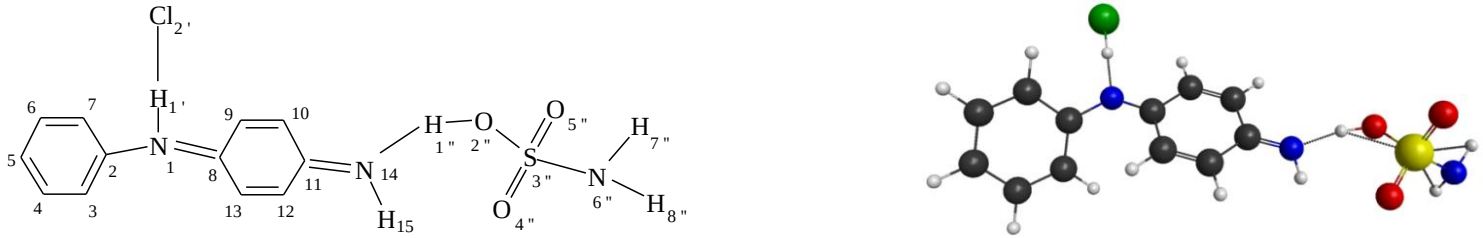

**ES-SA**

**(**ES-SA- (ES+SA) = -415.432 kJ/mole)

C-Black; H-Hydrogen; O- Red; N-Blue;Cl-Green; S-Yellow.

ISSN PRINT 2319 1775 Online 2320 7876
Research paper  UGC CARE Listed ( Group -I) Journal Volume 10, Iss 4, 2021

**Figure 2 : MO Diagram**

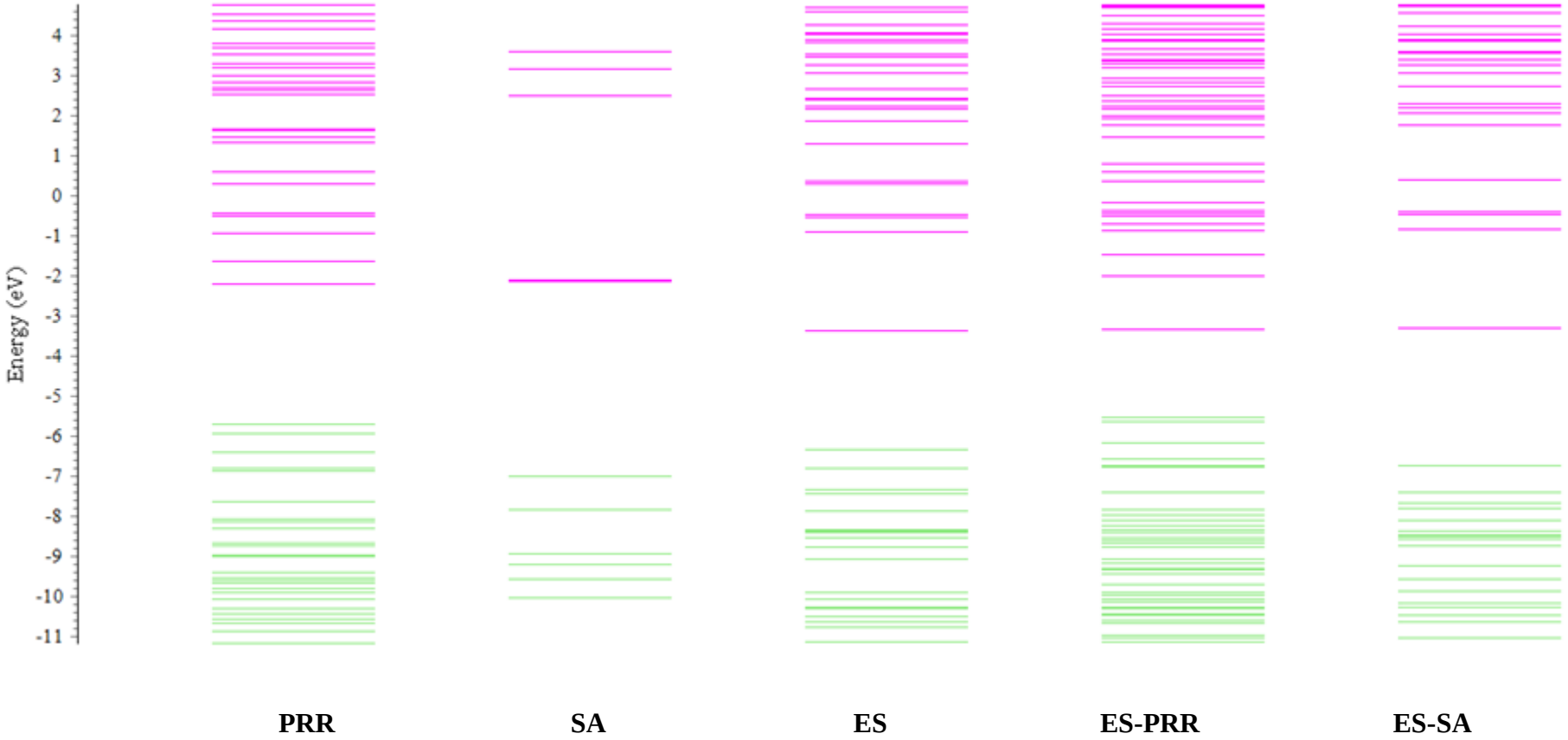


**Figure 3: MO Number, Name, Energy(eV) and AO Contribution to MO**

ISSN PRINT 2319 1775 Online 2320 7876
Research paper  UGC CARE Listed ( Group -I) Journal Volume 10, Iss 4, 2021

**PRR**

113-HOMO (-5.704)
$C_{16''}$-1$p_z$; $N_{14''}$-1$p_y$

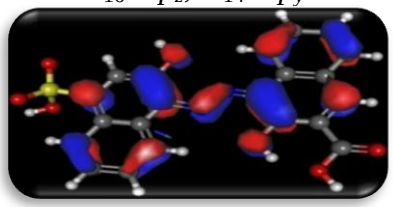

114-LUMO (-2.177)
$C_{23''}$-1$p_z$; $N_{15''}$-1$p_y$

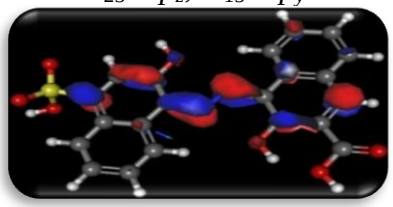

**SA**

25-HOMO (-6.977)
$O_{5''}$-1$p_y$; $O_{4''}$-1$p_x$

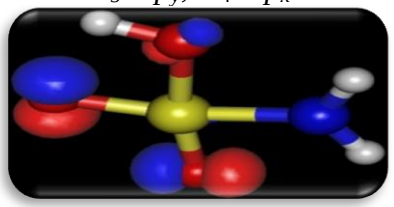

26-LUMO (-2.125)
$S_{3''}$-2$p_z$; $O_{5''}$-1$p_z$

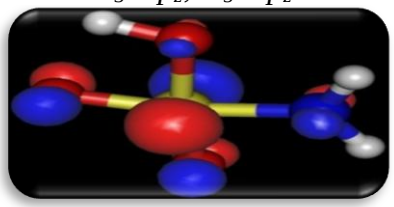

**ES-PRR**

170-HOMO (-5.529)
$N_{15''}$-1$p_x$; $N_{14''}$-1$p_x$

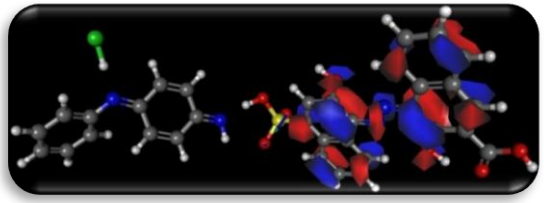

171-LUMO (-3.323)
$N_1$-1$p_z$; $N_{14}$-1$p_z$

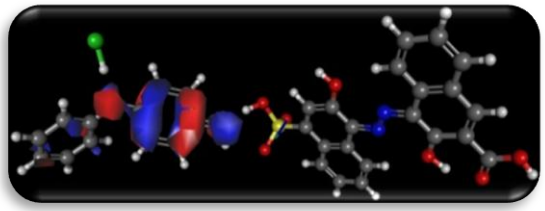

**ES-SA**

73-HOMO-9(-8.544)
$O_{4''}$-1$p_x$; $N_{14}$-1$p_y$

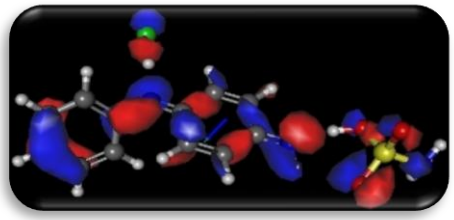

75-HOMO-7 (-8.471)
$C_{13}$-1$p_z$; $C_{12}$-1$p_z$

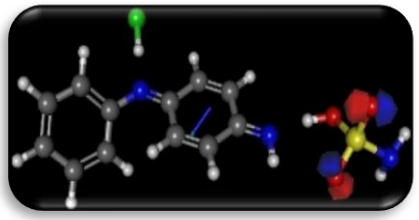

82-HOMO (-6.732)
$N_1$-1$p_y$; $C_2$-1$p_y$

83-LUMO (-3.279)
$N_7$-1$p_z$; $N_{14}$-1$p_z$

ISSN PRINT 2319 1775 Online 2320 7876
Research paper  UGC CARE Listed ( Group -I) Journal Volume 10, Iss 4, 2021

## Table 1: Structural Parameters

| Atom Pair | Bond Length (Å) | | Atom Pair | Bond Angle (°) | | Atom Pair | Dihedral Angle (°) | |
|---|---|---|---|---|---|---|---|---|
| | ES-PRR | ES-SA | | ES-PRR | ES-SA | | ES-PRR | ES-SA |
| $H_{1'}$-$Cl_{2'}$ | 1.3538 | 1.3535 | $Cl_{2'}$-$H_{1'}$-$N_1$ | 177.74 | 178.10 | $Cl_{2'}$-$H_{1'}$-$N_1$-$C_2$ | 103.81 | 102.80 |
| $H_{1'}$-$N_1$ | 1.6930 | 1.6935 | $H_{1'}$-$N_1$-$C_2$ | 114.64 | 114.51 | $H_{1'}$-$N_1$-$C_2$-$C_7$ | -38.32 | -39.68 |
| $N_1$-$C_2$ | 1.4031 | 1.4033 | $H_{1'}$-$N_1$-$C_8$ | 120.30 | 120.51 | $H_{1'}$-$N_1$-$C_8$-$C_9$ | -9.90 | -8.34 |
| $N_1$-$C_8$ | 1.3032 | 1.3030 | $N_1$-$C_2$-$C_3$ | 122.97 | 123.06 | $N_1$-$C_2$-$C_3$-$C_4$ | -176.50 | -176.68 |
| $C_2$-$C_3$ | 1.4085 | 1.4082 | $N_1$-$C_2$-$C_7$ | 117.46 | 117.37 | $N_1$-$C_2$-$C_7$-$C_6$ | 177.99 | 178.29 |
| $C_2$-$C_7$ | 1.4073 | 1.4070 | $C_2$-$C_3$-$C_4$ | 119.98 | 119.98 | $C_2$-$N_1$-$C_8$-$C_{13}$ | -9.65 | -8.92 |
| $C_3$-$C_4$ | 1.3930 | 1.3929 | $C_3$-$C_4$-$C_5$ | 120.39 | 120.38 | $C_2$-$C_3$-$C_4$-$C_5$ | 0.23 | -0.34 |
| $C_4$-$C_5$ | 1.3961 | 1.3961 | $C_6$-$C_7$-$C_2$ | 120.03 | 120.04 | $C_3$-$C_2$-$N_1$-$C_8$ | -46.09 | -46.58 |
| $C_6$-$C_7$ | 1.3907 | 1.3907 | $C_7$-$C_2$-$C_3$ | 119.35 | 119.36 | $C_4$-$C_3$-$C_2$-$C_7$ | -2.06 | -2.03 |
| $C_8$-$C_{13}$ | 1.4672 | 1.4673 | $C_8$-$N_1$-$C_2$ | 125.02 | 124.96 | $C_6$-$C_7$-$C_2$-$C_3$ | 3.25 | 3.34 |
| $C_9$-$C_{10}$ | 1.3472 | 1.3472 | $C_9$-$C_{10}$-$C_{11}$ | 121.32 | 121.30 | $C_8$-$C_{13}$-$C_{12}$-$C_{11}$ | 0.00 | 0.00 |
| $C_{10}$-$C_{11}$ | 1.4640 | 1.4641 | $C_{10}$-$C_{11}$-$C_{12}$ | 117.06 | 117.04 | $C_9$-$C_{10}$-$C_{11}$-$C_{12}$ | -1.21 | -1.66 |
| $C_{11}$-$C_{12}$ | 1.4678 | 1.4681 | $C_{11}$-$C_{12}$-$C_{13}$ | 121.71 | 121.75 | $C_{10}$-$C_{11}$-$C_{12}$-$C_{13}$ | 2.37 | 2.73 |
| $C_{11}$-$N_{14}$ | 1.2909 | 1.2909 | $C_{12}$-$C_{13}$-$C_8$ | 120.98 | 120.94 | $C_{11}$-$H_{15}$-$N_{14}$-$H_{1''}$ | -176.49 | 175.96 |
| $C_{12}$-$C_{13}$ | 1.3478 | 1.3475 | $C_{13}$-$C_8$-$N_1$ | 125.39 | 125.35 | $C_{12}$-$C_{11}$-$N_{14}$-$H_{15}$ | 2.06 | 0.00 |
| $N_{14}$-$H_{15}$ | 1.0233 | 1.0234 | $N_{14}$-$C_{11}$-$C_{12}$ | 123.31 | 123.33 | $C_{12}$-$C_{13}$-$C_8$-$N_1$ | 180.00 | 180.00 |
| $N_{14}$-$H_{1''}$ | 1.6087 | 1.6516 | | | | $C_{13}$-$C_{12}$-$C_{11}$-$N_{14}$ | -179.04 | -178.56 |

  

## Table 2: Mulliken's Atomic Charge Density

| ES-PRR | | ES-SA | |
|---|---|---|---|
| **Atom** | **Charge** | **Atom** | **Charge** |
| $H_{1'}$ | 0.1773 | $H_{1'}$ | 0.1773 |
| $Cl_{2'}$ | -0.2942 | $Cl_{2'}$ | -0.2945 |
| $N_1$ | -0.6016 | $N_1$ | -0.6022 |
| $C_2$ | 0.2486 | $C_2$ | 0.2480 |
| $C_3$ | -0.0976 | $C_3$ | -0.0973 |
| $C_4$ | -0.0958 | $C_4$ | -0.0958 |
| $C_5$ | -0.0752 | $C_5$ | -0.0756 |
| $C_6$ | -0.0916 | $C_6$ | -0.0915 |
| $C_7$ | -0.0915 | $C_7$ | -0.0907 |
| $C_8$ | 0.3327 | $C_8$ | 0.3334 |
| $C_9$ | -0.0985 | $C_9$ | -0.0991 |
| $C_{10}$ | -0.0753 | $C_{10}$ | -0.0733 |
| $C_{11}$ | 0.3379 | $C_{11}$ | 0.3332 |
| $C_{12}$ | -0.1091 | $C_{12}$ | -0.1095 |
| $C_{13}$ | -0.0903 | $C_{13}$ | -0.0910 |
| $N_{14}$ | -0.6402 | $N_{14}$ | -0.6364 |
| $H_{15}$ | 0.2856 | $H_{15}$ | 0.2830 |

## Table 3: Dipole moment (D)

| | $\mu_x$ | $\mu_y$ | $\mu_z$ | $\mu_{Total}$ |
|---|---|---|---|---|
| PRR | 2.2329 | -2.2320 | -1.3526 | 3.4347 |
| ES-PRR | 1.7098 | 1.2034 | -6.7523 | 7.0686 |
| SA | -2.3604 | 2.8645 | 0.0000 | 3.7117 |
| ES-SA | 3.5881 | -4.4120 | 2.3359 | 6.1479 |

## Table 4: TDDFT

**ES-SA**

| Wave Length (nm) | Oscillatory Strength | Orbital | % Contribution |
|---|---|---|---|
| 437.6 | 0.2763 | 82a → 83a | 77.99 |
| 309 | 0.2051 | 75a → 83a | 46.02 |
| 297.2 | 0.3148 | 73a → 83a<br>75a → 83a | 31.82<br>45.12 |

ISSN PRINT 2319 1775 Online 2320 7876
Research paper  UGC CARE Listed ( Group -I) Journal Volume 10, Iss 4, 2021

## Table 5: Frontier Molecular Orbital

| | eV | | | | | | | | $Q^{Max}$ |
|---|---|---|---|---|---|---|---|---|---|
| | **Band Gap** | **Ionisation potential** | **Electron affinity** | **Electronic chemical potential** | **Chemical hardness** | **Global softness** | **Electrophilic index** | **EN** | |
| PRR | 3.5 | 5.7 | 2.2 | -3.9 | 1.8 | 0.6 | 13.7 | 3.9 | 2.2 |
| SA | 4.9 | 7.0 | 2.1 | -4.6 | 2.4 | 0.4 | 25.1 | 4.6 | 1.9 |
| ES-PRR | 2.2 | 5.5 | 3.3 | -4.4 | 1.1 | 0.9 | 10.8 | 4.4 | 4.0 |
| ES-SA | 3.5 | 6.7 | 3.3 | -5.0 | 1.7 | 0.6 | 21.6 | 5.0 | 2.9 |

## Table 6: Polarisability (Au)

| Axis | PRR | ES-PRR | SA | ES-SA |
|---|---|---|---|---|
| $\mu_Z$ | -0.532 | -2.66 | $2.94\times 10^{-15}$ | 0.919 |
| $\alpha_{XZ}$ | -6.81 | 23.0 | $1.21\times 10^{-11}$ | -25.7 |
| $\alpha_{YZ}$ | -0.837 | -18.0 | $2.78\times 10^{-11}$ | -1.51 |
| $\alpha_{ZZ}$ | 1.00 | 269 | 19.00 | 103 |
| $\beta_{XZZ}$ | 11.4 | 685 | -0.699 | -8.48 |
| $\beta_{YZZ}$ | -6.77 | 12.9 | 1.62 | 22.8 |
| $\beta_{ZZZ}$ | 0.548 | -153 | $-1.05\times 10^{-09}$ | -45.0 |
| $\gamma_{ZZZZ}$ | 477 | $3.77\times 10^{04}$ | 212 | 1460 |

ISSN PRINT 2319 1775 Online 2320 7876
Research paper  UGC CARE Listed ( Group -I) Journal Volume 10, Iss 4, 2021

# Table 7: Conductance

## ES-SA

| Mole Fraction of ES | Conductance S/cm |
|---|---|
| 1 | 0.4910 |
| 0.7771 | 0.1797 |
| 0.6354 | 0.2491 |
| 0.5375 | 0.3020 |
| 0.4657 | 0.3579 |

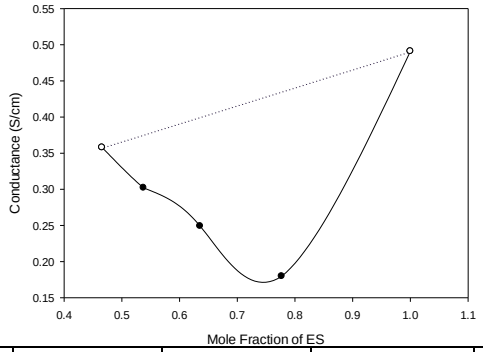


| | R | $y_0$ | a | b |
|---|---|---|---|---|
| **Ideal** | 1.0 | 0.2419 | 0.2491 | - |
| **Real** | 0.9690 | 1.7714 | -4.4731 | 3.1836 |

## ES-PRR

| Mole Fraction of ES | Conductance S/cm |
|---|---|
| 1 | 0.4910 |
| 0.9403 | 0.2568 |
| 0.8873 | 0.1132 |
| 0.8399 | 0.0840 |
| 0.7974 | 0.0461 |

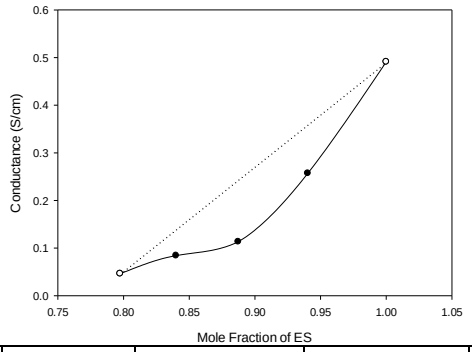


| | R | $y_0$ | a | b |
|---|---|---|---|---|
| **Ideal** | 1.0 | -1.7048 | 2.1958 | - |
| **Real** | 0.9976 | 7.9307 | -19.4617 | 12.0197 |

## ES-BCG

| Mole Fraction of ES | Conductance S/cm |
|---|---|
| 1.0000 | 0.4910 |
| 0.9616 | 0.0695 |
| 0.9261 | 0.0563 |
| 0.8931 | 0.0397 |
| 0.8624 | 0.0337 |

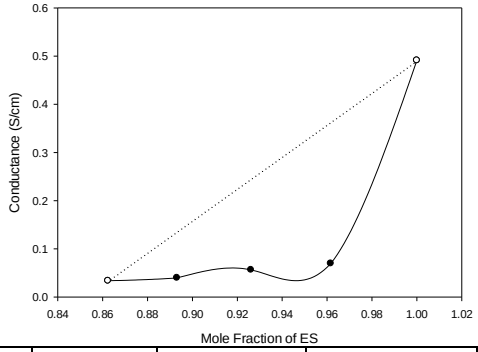


| | R | $y_0$ | a | b |
|---|---|---|---|---|
| **Ideal** | 1.0 | -2.8318 | 3.3228 | - |
| **Real** | 0.9526 | 39.8639 | -88.3774 | 48.9683 |